

Enhancement of microorganism swimming speed in active matter

Harsh Soni¹, Robert A. Pelcovits², and Thomas R. Powers^{1,2}
¹*School of Engineering, Brown University, Providence, RI 02912 USA and*
²*Department of Physics, Brown University, Providence, RI 02012 USA*
(Dated: June 8, 2021)

We study a swimming undulating sheet in the isotropic phase of an active nematic liquid crystal. Activity changes the effective shear viscosity, reducing it to zero at a critical value of activity. Expanding in the sheet amplitude, we find that the correction to the swimming speed due to activity is inversely proportional to the effective shear viscosity. Our perturbative calculation becomes invalid near the critical value of activity; using numerical methods to probe this regime, we find that activity enhances the swimming speed by an order of magnitude compared to the passive case.

PACS numbers: 47.63.Gd, 82.70.-y, 47.57.Lj

Recent years have seen many advances in the study of swimming at the micron scale in viscous fluids [1], such as the creation of artificial microswimmers [2–4], measurements of the flows induced by single swimmers [5–7], and the development of hydrodynamic theories [8–10] and simulations [11–13]. The field has expanded to include swimmers in non-Newtonian fluids, such as viscoelastic polymer solutions [14–19] and liquid crystals [20–22]. All of these studies involve passive fluids, in which the energy that drives the flow is added by the internal motors of the swimmer or an external source such as a rotating magnetic field. In active fluids, on the other hand, the energy that drives the flow is added to the system at the level of the microscopic constituents of the fluid [23]. For example, a suspension of molecular motors and cytoskeletal filaments shows spontaneous flows due to the consumption of ATP in the suspension by the molecular motors [24, 25]. It is natural to ask if an active fluid can do work on a swimmer, causing it to swim faster than it would in a passive fluid with the same stroke. In this Letter we investigate this question with the Taylor model of a waving sheet [26] in the isotropic phase of an active nematic liquid crystal (Fig 1).

We use the Taylor sheet because it is one of the simplest models for a flagellated swimmer for which analytical calculations of swimming speed are possible. The isotropic state of the fluid is also chosen for simplicity. Below a critical activity, the undisturbed stable state of the active liquid crystal is isotropic with no flow. The motion of a swimmer induces flows around the swimmer which in turn lead to local order; the simple nature of the base state allows us to treat the swimmer problem perturbatively. An unconfined active nematic in the nematic phase is unstable to spontaneous flow at any value of activity [27], making an analytic approach difficult.

We model the isotropic phase of an active nematic by adding activity to de Gennes’ hydrodynamic model [28–30] for the isotropic phase of a passive nematic fluid. The governing equations are similar to those used in other studies of active matter [31–33]. A striking feature of the active isotropic phase of extensile prolate particles (or

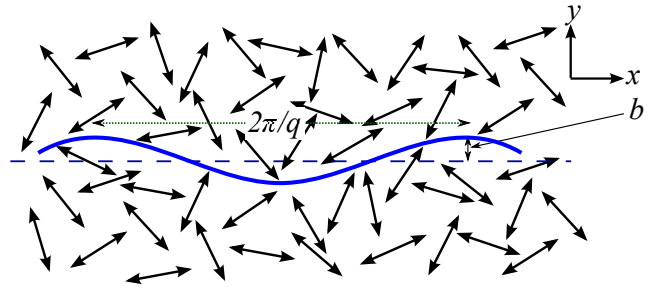


FIG. 1. (Color online.) A Taylor sheet (blue wavy line) with wavenumber q and amplitude b swimming in an active nematic liquid fluid in the isotropic phase. The double headed arrows are the active nematic molecules.

contractile oblate particles) is that activity reduces the effective shear viscosity (Fig. 2) [31]. In fact, numerical and experimental studies have given evidence for a “superfluid” state in which the apparent viscosity vanishes for sufficiently large activity [34–38]. We find that the swimming speed for a small-amplitude Taylor sheet in our active medium is inversely proportional to the effective shear viscosity. Since our perturbative calculation breaks down when the effective shear viscosity gets too small, we use numerical finite-element methods to show that the swimming speed for small effective viscosity can be an order of magnitude larger than the speed in a passive medium for the same stroke. The outline for the remainder of the Letter is as follows. After introducing the governing equations, we find the critical value of the activity at which the quiescent isotropic state becomes unstable. Then we calculate the swimming speed using perturbation theory, which is valid for a value of activity that is sufficiently smaller than the critical value for instability. Finally we numerically calculate the flow, order parameter field, and swimming speed, again assuming the activity is such that the quiescent isotropic state is stable.

To motivate the governing equations, we begin with the nematic degrees of freedom. For simplicity we assume a one-dimensional deformation of the sheet, with

no variation in the spatial direction perpendicular to the plane of the Fig. 1. Thus the the local nematic ordering is characterized by a symmetric traceless order parameter tensor $Q_{\alpha\beta}$, with $\alpha, \beta = x, y$. To leading order in $Q_{\alpha\beta}$, the Landau-de Gennes free energy density is [29]

$$\mathcal{F} = \frac{A}{2} Q_{\alpha\beta} Q_{\alpha\beta}, \quad (1)$$

where we sum over repeated indices and $A > 0$ in the isotropic phase. Frank elasticity can be neglected in the isotropic phase as can higher order terms in $Q_{\alpha\beta}$ (note that a cubic term is identically zero in two dimensions). Strictly speaking, a quartic term should be included since the perturbative calculation of the swimming speed requires an expansion to second order in the swimmer amplitude. But the qualitative effect of retaining this term in the calculation is only to slightly change the shape of the potential defined by \mathcal{F} , leading to a slight change in the numerical factors in the expression for swimming speed. Thus the molecular field is $\Phi_{\alpha\beta} \equiv -\partial\mathcal{F}/\partial Q_{\alpha\beta} = -AQ_{\alpha\beta}$ in the isotropic phase. The equilibrium stress is the Ericksen stress, $\sigma_{\alpha\beta}^e = \mathcal{F}\delta_{\alpha\beta} - \partial\mathcal{F}/\partial(\partial_\beta Q_{\mu\nu})\partial_\alpha Q_{\mu\nu}$ [28, 39].

The rate of entropy production per volume is [29]

$$T\dot{S} = \sigma'_{\alpha\beta} e_{\alpha\beta} + \Phi_{\alpha\beta} R_{\alpha\beta}, \quad (2)$$

where T is temperature, S is entropy per volume, $\sigma'_{\alpha\beta}$ is the viscous stress tensor, $e_{\alpha\beta} = (\partial_\alpha v_\beta + \partial_\beta v_\alpha)/2$ is the strain rate tensor, v_α is the velocity field, and $R_{\alpha\beta}$ is the rate of change of $Q_{\alpha\beta}$ relative to the local rate of rotation $\omega_{\alpha\beta} = (\partial_\alpha v_\beta - \partial_\beta v_\alpha)/2$ of the background fluid,

$$R_{\alpha\beta} = \partial_t Q_{\alpha\beta} + \mathbf{v} \cdot \nabla Q_{\alpha\beta} + \omega_{\alpha\gamma} Q_{\gamma\beta} - Q_{\alpha\gamma} \omega_{\gamma\beta}. \quad (3)$$

Following de Gennes [28], we take the forces in the entropy source to be the molecular field $\Phi_{\alpha\beta}$ and the viscous stress tensor $\sigma'_{\alpha\beta}$, and the corresponding fluxes to be $e_{\alpha\beta}$ and $R_{\alpha\beta}$. Assuming that the forces are linear functions of the fluxes, the phenomenological equations relating the forces to the fluxes are

$$\sigma'_{\alpha\beta} = 2\eta e_{\alpha\beta} + 2(\mu + \mu_1)R_{\alpha\beta} + aQ_{\alpha\beta} \quad (4)$$

$$\Phi_{\alpha\beta} = 2\mu e_{\alpha\beta} + \nu R_{\alpha\beta}, \quad (5)$$

where η is the shear viscosity, μ and μ_1 couple shear and alignment, and ν is the rotational viscosity. Note that η , μ , μ_1 , and ν have units of viscosity, and a and A have units of a modulus. We neglect higher-order terms such as $Q_{\alpha\gamma} e_{\gamma\delta} Q_{\delta\beta}$ since the magnitude of the order parameter is small in the isotropic phase. The coefficients μ_1 and a arise from activity. When $a = 0$ and $\mu_1 = 0$, the Onsager reciprocal relations [40] hold, and the rate of entropy production is positive, implying $\eta\nu - 2\mu^2 > 0$. Thus, the active parameter μ_1 determines the degree of violation of the Onsager relations, and, when it is sufficiently positive, can lead to a negative rate of entropy production.

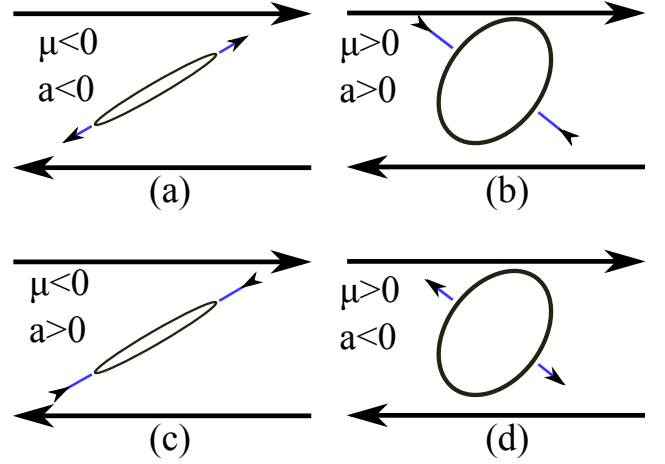


FIG. 2. (Color online.) Effect of activity a on the effective shear viscosity of the nematic fluid. The large arrows represent the shear flow and the small arrows represent the forces due to activity. Extensile prolate particles (a) and contractile oblate particles (b) reduce the shear viscosity [31]. (Note that the force axis always assumed along the particle axis of symmetry.) Contractile prolate particles (c) and extensile oblate particles (d) increase the shear viscosity [31].

The active stress is $aQ_{\alpha\beta}$ [31], with $a < 0$ for extensile particles and $a > 0$ for contractile particles. The coupling μ controls the orientation of the particles in shear flow, leading to shear birefringence. For example, nematic order develops in a weak steady shear flow, with $Q_{\alpha\beta} = -(2\mu/A)e_{\alpha\beta}$ to first order in the strain rate [28]. Note that independent of the value of μ_1 , particles with $\mu < 0$, such as prolate ellipsoidal particles, align along the shear flow, and particles with $\mu > 0$, such as oblate ellipsoidal particles, align opposite to the shear flow (Fig. 2).

The governing equations are the director equation Eq. (5) and the force balance equation $\partial_\beta \sigma_{\alpha\beta} = 0$, with $\sigma_{\alpha\beta} = -p\delta_{\alpha\beta} + \sigma_{\alpha\beta}^e + \sigma'_{\alpha\beta}$. We define the effective viscosity η_{eff} and the effective coupling μ_{eff} by using Eq. (5) to eliminate $Q_{\alpha\beta}$ from the stress, Eq. (4), to find $\sigma'_{\alpha\beta} = 2\eta_{\text{eff}}e_{\alpha\beta} + 2\mu_{\text{eff}}R_{\alpha\beta}$, where

$$\eta_{\text{eff}} = \eta - \frac{\mu a}{A} \quad (6)$$

$$\mu_{\text{eff}} = \mu + \mu_1 - \frac{\nu a}{2A}. \quad (7)$$

Thus, activity gives rise to an effective shear viscosity η_{eff} which vanishes at a critical value of the activity $a_c = A\eta/\mu$.

Next we turn to the linear stability analysis of the state with $v_\alpha = 0$ and $Q_{\alpha\beta} = 0$, with no swimmer or other confining boundaries. To linear order, the force balance equation is

$$-\partial_\alpha p + 2\eta_{\text{eff}}\partial_\beta e_{\alpha\beta} + 2\mu_{\text{eff}}\partial_\beta \dot{Q}_{\alpha\beta} = 0, \quad (8)$$

where $\dot{Q}_{\alpha\beta} = \partial_t Q_{\alpha\beta}$. The pressure p is determined by the incompressibility constraint, $\partial_\alpha v_\alpha = 0$. It is convenient

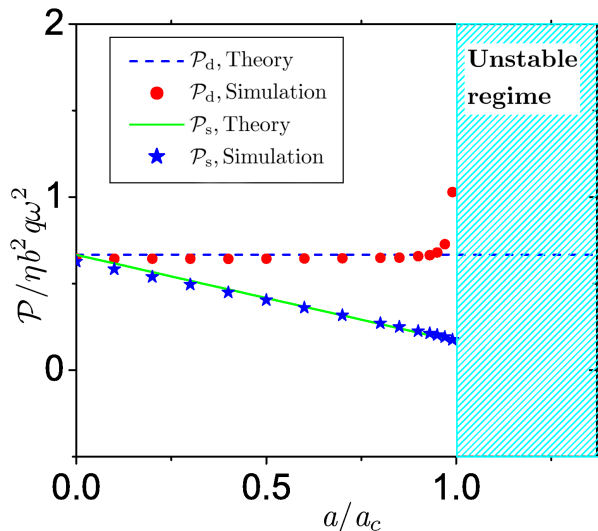


FIG. 3. (Color online.) Dimensionless rate of working \mathcal{P}_s of the swimmer (green line from theory, Eq. 17, blue stars from simulations) vs. dimensionless activity a/a_c , and dimensionless rate of dissipation of energy \mathcal{P}_d (blue dashed line from theory, red dots from simulation) vs. dimensionless activity a/a_c . The parameters used are $\epsilon = bq = 0.1$, $\mu = \eta = \nu/3$, $A = \nu\omega$ and $\mu_1 = 0$.

to enforce incompressibility with the stream function ψ , defined so that $\mathbf{v} = \nabla \times \psi \hat{\mathbf{z}}$. Also, in two dimensions, the tensor order parameter $Q_{\alpha\beta}$ is related to the scalar order parameter S and the director \mathbf{n} via $Q_{\alpha\beta} = S(2n_\alpha n_\beta - \delta_{\alpha\beta})$. The linearized equations for the stream function and the order parameter are

$$-\Delta^2 \psi + 2 \frac{\mu_{\text{eff}}}{\eta_{\text{eff}}} \left[(\partial_x^2 - \partial_y^2) \dot{Q}_{xy} - 2 \partial_x \partial_y \dot{Q}_{xx} \right] = 0 \quad (9)$$

$$2\mu \partial_x \partial_y \psi + A Q_{xx} + \nu \dot{Q}_{xx} = 0 \quad (10)$$

$$-\mu (\partial_x^2 - \partial_y^2) \psi + A Q_{xy} + \nu \dot{Q}_{xy} = 0, \quad (11)$$

where $\nabla = \partial_x^2 + \partial_y^2$.

For perturbations of the velocity and order parameter tensor proportional to $\exp[i(\mathbf{q} \cdot \mathbf{x} - \sigma t)]$, the characteristic equation for this problem yields two roots [41],

$$\sigma_1 = -A/\nu \quad (12)$$

$$\sigma_2 = -A\eta_{\text{eff}}/(\eta_{\text{eff}}\nu - 2\mu\mu_{\text{eff}}). \quad (13)$$

The roots are independent of the direction of \mathbf{q} since the base state is isotropic. There are only two roots since the assumption of zero Reynolds number has eliminated $\partial_t v_\alpha$ from the governing equations. The first root σ_1 is always positive; inserting $\exp[i(\mathbf{q} \cdot \mathbf{x} - \sigma_1 t)]$ into Eq. (10) or Eq. (11) reveals that this mode has no flow, with the director \mathbf{n} parallel to \mathbf{q} for all \mathbf{x} and all t , and the scalar order parameter relaxing to zero with rate A/ν .

The second root corresponds to a mode in which there is a shear flow with the velocity perpendicular to \mathbf{q} (due to incompressibility $\mathbf{q} \cdot \mathbf{v} = 0$), with \mathbf{n} along the flow.

The numerator in Eq. (13) is precisely the quantity that determines whether or not the entropy production $T\dot{S}$ is positive. If μ_1 is small enough that $\eta_{\text{eff}}\nu - 2\mu\mu_{\text{eff}} > 0$, then the isotropic state is unstable when $\eta_{\text{eff}} < 0$, i.e. $a > a_c = A\eta/\mu$ for positive μ (Fig. 2b), or $a < a_c = A\eta/\mu$ for negative μ (Fig. 2a). The quiescent isotropic state is unstable against shear flow and local ordering when the shear-induced orientation of the particles leads to greater shear flow, as in Figs. 2a and 2b.

We now consider a Taylor swimmer with $y = h(x, t) \equiv b \cos(qx - \omega t)$ (Fig. 1) in the stable phase of an isotropic active nematic. Our approach is the same as Lauga's calculation for a dilute polymer solution [14]. To calculate the swimming speed of the sheet, we work in the rest frame of the swimmer and solve the governing equations (4) and (5) with no-slip boundary conditions on the velocity at the swimmer, $\mathbf{v}(x, y = h) = \partial_t h(x, t) \hat{\mathbf{y}}$. The unknown velocity at $y \rightarrow \infty$ is the negative of swimming velocity U . No boundary conditions are imposed on the order parameter because we have disregarded the Frank energy. We assume that $\epsilon = bq \ll 1$ and expand in powers of ϵ , so that e.g. $\psi = \epsilon\psi^{(1)} + \epsilon^2\psi^{(2)}$. To first order in ϵ the equations (9–11) yield

$$\psi^{(1)} = (\omega/q^2)(1 + qy)e^{-qy} \cos(qx - \omega t) \quad (14)$$

$$Q_{xx}^{(1)} = \frac{-2qy\omega\mu e^{-qy}}{A^2 + \omega^2\nu^2} [\omega\nu \cos(qx - \omega t) + A \sin(qx - \omega t)]$$

$$Q_{xy}^{(1)} = \frac{-2qy\omega\mu e^{-qy}}{A^2 + \omega^2\nu^2} [A \cos(qx - \omega t) - \omega\nu \sin(qx - \omega t)].$$

The velocity field is the same as the Stokes flow found by Taylor [26] for a Newtonian fluid, and the order parameter is independent of the activity. Note that the direction of \mathbf{n} is independent of y to first order in ϵ , since the ratio $Q_{xy}^{(1)}/Q_{xx}^{(1)}$ is independent of y .

The power P_s supplied by the swimmer is equal to the sum of the rate of change of the free energy and the net power dissipated in the fluid, $P_s = dF/dt + P_f$, where $F = \int d^3x \mathcal{F}$ and

$$P_s = - \int \left[v_\alpha \sigma_{\alpha\beta} + \frac{\partial \mathcal{F}}{\partial (\partial_\beta Q_{\mu\nu})} \frac{dQ_{\mu\nu}}{dt} \right] N_\beta dS \quad (15)$$

$$P_f = \int \left[e_{\alpha\beta} (\sigma_{\alpha\beta} - \sigma_{\alpha\beta}^e) + \Phi_{\alpha\beta} \frac{dQ_{\alpha\beta}}{dt} \right] d^3x. \quad (16)$$

Here $dQ_{\alpha\beta}/dt = \partial_t Q_{\alpha\beta} + v_\gamma \partial_\gamma Q_{\alpha\beta}$, dS is area element of the swimmer, and $\hat{\mathbf{N}}$ is the outward-pointing normal to the swimmer. Note that the net power dissipated in the fluid may be negative due to activity. The first-order solutions allow us to calculate the leading order rate of working of the swimmer per unit area of the sheet,

$$\mathcal{P}_s \approx b^2 q \omega^2 \left[\eta_{\text{eff}} - \frac{2\nu\mu\mu_{\text{eff}}\omega^2}{A^2 + \nu^2\omega^2} \right] \quad (17)$$

(note that $P_s = \int dS \mathcal{P}_s$). The power supplied by the swimmer decreases linearly with activity a (Fig. 3, green

solid line). The fluid does net positive work on the swimmer when $a > a_0 = a_c + [\eta\nu - 2\mu(\mu + \mu_1)]\omega^2/(A\mu)$. The value of a_0 can be less than a_c and in the regime where our perturbative calculation is valid when μ_1 is sufficiently large and positive. We denote the power dissipated in the fluid per unit area of the sheet by $\mathcal{P}_d \equiv \mathcal{P}_f(a = 0, \mu_1 = 0)$; \mathcal{P}_d is positive and independent of activity (Fig. 3, blue dashed line), and to leading order is given by (17) with η_{eff} replaced by η and μ_{eff} replaced by μ .

To find the swimming speed, it is convenient to write the time-average of the x -component of momentum balance in terms of the velocity and expand to second order in ϵ :

$$\eta_{\text{eff}} \frac{d^2}{dy^2} \langle v_x^{(2)} \rangle + 4e^{-2qy} (qy - 2) y q^2 \omega^3 \frac{2\mu\nu\mu_{\text{eff}}}{A^2 + \nu^2\omega^2} = 0. \quad (18)$$

Enforcing the no-slip boundary condition to second order leads to $\langle v_x^{(2)}(x, 0) \rangle = \omega/(2q)$. Solving for the flow leads to the swimming speed

$$U = \frac{c\epsilon^2}{2} \left[1 - \frac{2\nu\mu\mu_{\text{eff}}\omega^2}{\eta_{\text{eff}}(A^2 + \nu^2\omega^2)} \right], \quad (19)$$

where $c = \omega/q$ is the wave speed of the deformation of the swimmer, and we are using the convention that a positive U means the swimmer moves left in the laboratory frame. In the supplementary material [41] we show that the swimming speed of a two-dimensional squirmer has the same dependence on frequency ω and material parameters ν , μ , μ_{eff} , η_{eff} , and A . The swimming speed diverges when $a \rightarrow a_c$ since the effective shear viscosity vanishes at the critical activity, indicating a breakdown of the perturbative calculation. Analyzing the form of the next order terms reveals that they are of the order of $\epsilon^4/(a_c - a)^3$, indicating that the perturbative approach requires $\epsilon^2 \ll (a_c - a)^2$. Also, when $a < a_c$, U is positive. Thus as long as the fluid is stable, activity cannot make the swimmer swim in the direction of the propagating waves.

To go beyond the restriction $\epsilon^2 \ll (a_c - a)^2$, we solve the force balance equation $\partial_\beta \sigma_{\alpha\beta} = 0$ and the director equation (5) numerically using the COMSOL Multiphysics® software [42]. We scale length by $1/q$ and time by $1/\omega$, and choose $\epsilon = 0.1$, $\mu = \eta = \nu/3$, $A = \nu\omega$ and $\mu_1 = 0$. To approximate the infinite system, we choose the size of the simulation box much larger than the decay length $1/q$. The simulation box has dimensions 32π and 60 along the x and y directions, respectively, with periodic boundary conditions along the x direction. The Taylor sheet is represented by the top wall (Fig. 5), which deforms and has a no-slip boundary condition. In order to ensure that the sheet is subjected to no net force along the x direction, we choose the slip boundary condition $\sigma_{xy} = 0$ on the bottom wall. More

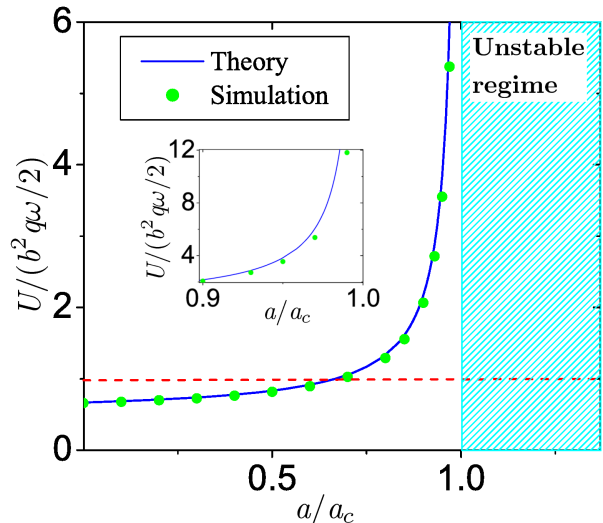


FIG. 4. (Color online.) Dimensionless swimming speed $U/(b^2 q \omega / 2)$ vs. dimensionless activity a/a_c from theory, Eq. 19, (blue line) and simulations (green dots). The parameters used are the same as in Fig. 3. The inset shows the critical region $a \approx a_c$.

details of the numerical method are discussed in the supplementary material [41].

Figure 4 shows the numerically calculated U vs. a_0 for $a < a_c$. The speed U increases with a monotonically, with good agreement between the simulations and theory when $a < 0.9a_c$. At $a = 0.99a_c$, the swimming speed is enhanced up to around 12 times the swimming speed of the Taylor case (see the inset of Fig. 4). We do not perform numerical studies much closer to the critical activity because the decay length increases as $a \rightarrow a_c$, requiring a larger simulation box. In Fig. 5, we show the flow profile around the Taylor sheet superimposed with the heat map of the order parameter $S = \sqrt{Q_{xx}^2 + Q_{yy}^2}$. The figure illustrates flow birefringence: S attains its greatest values in the regions where shear is greatest.

The numerically calculated power exerted by the swimmer and power dissipated in the fluid are shown in Fig. 3. The power exerted by the swimmer decreases with increasing activity (blue stars) whereas the rate of dissipation increases with increasing activity (red dots). When $a = 0$, the power exerted by the swimmer equals the power dissipated in the fluid. However in the presence of activity, the swimmer does not work as hard, since part of the power generated by activity contributes to work on the swimmer, and part is dissipated in the fluid.

We have studied the swimming of a model microorganism in the isotropic phase of an active nematic liquid crystal. As activity approaches the critical value at which the quiescent fluid is unstable to spontaneous shear flow, the swimming speed increases dramatically. An important extension of this work would be to study swimmers in the unsteady regime above the critical activity.

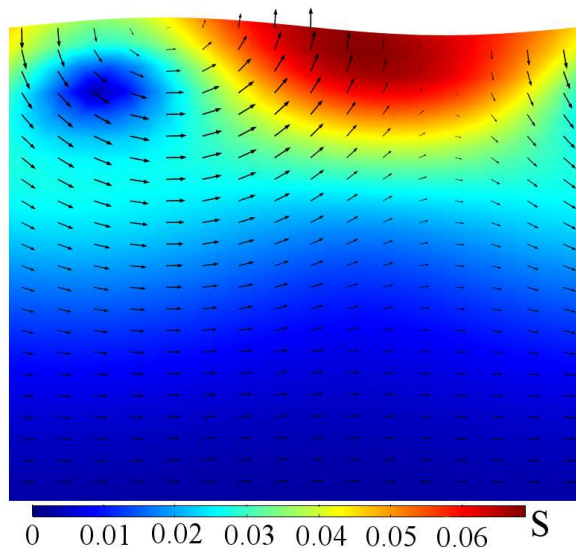


FIG. 5. (Color online.) Flow profile (black arrows) around the Taylor sheet superimposed with the heat map for the order parameter $S = \sqrt{Q_{xx}^2 + Q_{xy}^2}$ at $a_0 = 0.99$, $\epsilon = bq = 0.1$, $\mu = \eta = \nu/3$, $A = \nu\omega$ and $\mu_1 = 0$. Here the size of the simulation box is $16\pi \times 60$ but we only show the portion of size $2\pi \times 20$.

We thank Aparna Baskaran, Ray Goldstein, David Henann, Oleg Lavrentovich, and Sriram Ramaswamy for helpful discussions. This work was supported in part by National Science Foundation Grant No. CBET-1437195 and National Science Foundation Grant MRSEC-1420382.

[1] E. Lauga and T. R. Powers, *Rep. Prog. Phys.* **72**, 096601 (2009).
[2] K. Ishiyama, M. Sendoh, A. Yamazaki, and K. I. Aral, *Sens. Actuators A* **91**, 141 (2001).
[3] R. Dreyfus, J. Baudry, M. L. Roper, M. Fermigier, H. A. Stone, and J. Bibette, *Nature* **437**, 862 (2005).
[4] A. Ghosh and P. Fischer, *Nano Lett.* **9**, 2243 (2009).
[5] J. Guasto, K. Johnson, and J. Gollub, *Phys. Rev. Lett.* **105**, 168102 (2010).
[6] K. Drescher, J. Dunkel, L. H. Cisneros, S. Ganguly, and R. E. Goldstein, *Proc. Natl. Acad. Sci. (USA)* **108**, 10940 (2011).
[7] R. E. Goldstein, *Ann. Rev. Fluid Mech.* **47**, 343 (2015).
[8] H. Stone and A. Samuel, *Phys. Rev. Lett.* **77**, 4102 (1996).
[9] A. Najafi and R. Golestanian, *J. Phys. Cond. Mat.* **17**, S1203 (2005).
[10] O. S. Pak and E. Lauga, in *Low-Reynolds-Number Flows: Fluid-Structure Interactions*, RSC Soft Matter Series, Vol. 4, edited by E. Duprat and H. A. Stone (The Royal Society of Chemistry, 2015) p. 100.
[11] C. Pozrikidis, *Boundary integral and singularity methods for linearized viscous flow* (Cambridge University Press,

Cambridge, 1992).
[12] S. Cortez, *SIAM J. Sci. Comput.* **23**, 1204 (2001).
[13] R. Cortez, L. Fauci, and A. Medovikov, *Phys. Fluids* **17**, 031504 (2005).
[14] E. Lauga, *Physics of Fluids* **19**, 083104 (2007).
[15] H. C. Fu, T. R. Powers, and C. W. Wolgemuth, *Phys. Rev. Lett.* **99**, 258101 (2007).
[16] J. Teran, L. Fauci, and M. Shelley, *Phys. Rev. Lett.* **104**, 038101 (2010).
[17] X. N. Shen and P. E. Arratia, *Phys. Rev. Lett.* **106**, 208101 (2011).
[18] B. Liu, T. R. Powers, and K. S. Breuer, *Proc. Natl. Acad. Sci. (USA)* **108**, 19516 (2011).
[19] S. E. Spagnolie, ed., *Complex Fluids in Biological Systems* (Springer, New York, 2015).
[20] S. Zhou, A. Sokolov, O. D. Lavrentovich, and I. S. Aranson, *Proc. Natl. Acad. Sci. USA* **111**, 1265 (2014).
[21] P. C. Mushenheim, R. R. Trivedi, H. H. Tuson, D. B. Weibel, and N. L. Abbott, *Soft Matter* **10**, 88 (2014).
[22] M. S. Krieger, S. E. Spagnolie, and T. R. Powers, *Phys. Rev. E* **90**, 052503 (2014).
[23] M. C. Marchetti, J. F. Joanny, S. Ramaswamy, T. B. Liverpool, J. Prost, M. Rao, and R. A. Simha, *Rev. Mod. Phys.* **85**, 1143 (2013).
[24] V. Schaller, C. Weber, C. Semmrich, E. Frey, and A. R. Bausch, *Nature* **467**, 73 (2010).
[25] T. Sanchez, D. T. N. Chen, S. J. DeCamp, M. Heymann, and Z. Dogic, *Nature* **491**, 431 (2012).
[26] G. Taylor, *Proceedings of the Royal Society of London A: Mathematical, Physical and Engineering Sciences* **209**, 447 (1951).
[27] L. Giomi, L. Mahadevan, B. Chakraborty, and M. F. Hagan, *Nonlinearity* **25**, 2245 (2012).
[28] P. G. de Gennes, *Physics Letters A* **30**, 454 (1969).
[29] P. G. de Gennes and J. Prost, *The physics of liquid crystals* (Clarendon Press Oxford University Press, Oxford New York, 1993).
[30] P. G. de Gennes, *Molecular Crystals and Liquid Crystals* **12**, 193 (1971).
[31] Y. Hatwalne, S. Ramaswamy, M. Rao, and R. A. Simha, *Phys. Rev. Lett.* **92**, 118101 (2004).
[32] D. Saintillan and M. J. Shelley, *Phys. Rev. Lett.* **100**, 178103 (2008).
[33] F. G. Woodhouse and R. E. Goldstein, *Phys. Rev. Lett.* **109**, 168105 (2012).
[34] M. E. Cates, S. M. Fielding, D. Marenduzzo, E. Orlandini, and J. M. Yeomans, *Phys. Rev. Lett.* **101**, 068102 (2008).
[35] A. Sokolov and I. S. Aranson, *Phys. Rev. Lett.* **103**, 148101 (2009).
[36] L. Giomi, T. B. Liverpool, and M. C. Marchetti, *Phys. Rev. E* **81**, 051908 (2010).
[37] J. Gachelin, G. Miño, H. Berthet, A. Lindner, A. Rouselet, and E. Clément, *Phys. Rev. Lett.* **110**, 268103 (2013).
[38] H. M. López, J. Gachelin, C. Douarche, H. Auradou, and E. Clément, *Phys. Rev. Lett.* **115**, 028301 (2015).
[39] F. Jülicher, S. W. Grill, and G. Salbreux, *Rep. Prog. Phys.* **81**, 076601 (2018).
[40] L. Onsager, *Phys. Rev.* **37**, 405 (1931).
[41] See Supplemental material at [] for more detail.
[42] COMSOL Multiphysics v. 5.2. www.comsol.com. COMSOL AB, Stockholm, Sweden.

Supplemental Material

Enhancement of microorganism swimming speed in active matter

Harsh Soni¹, Robert A. Pelcovits², and Thomas R. Powers^{1,2}

¹*School of Engineering, Brown University, Providence, RI 02912 USA and*

²*Department of Physics, Brown University, Providence, RI 02012 USA*

arXiv:1807.03390v1 [cond-mat.soft] 9 Jul 2018

I. STABILITY ANALYSIS

Our equations of motion are given by

$$-\partial_\alpha p + 2\eta\partial_\alpha e_{\beta\alpha} + 2(\mu + \mu_1)\partial_\alpha R_{\beta\alpha} + a\partial_\alpha Q_{\beta\alpha} = 0 \quad (1)$$

$$AQ_{\alpha\beta} + 2\mu e_{\alpha\beta} + \nu R_{\alpha\beta} = 0. \quad (2)$$

corresponding respectively to $\partial_\beta\sigma_{\alpha\beta} = 0$ with the Ericksen stress $\sigma_{\alpha\beta}^e = AQ_{\gamma\delta}Q_{\gamma\delta}\delta_{\alpha\beta}$ absorbed into pressure, and Eq. (5) (using $\Phi_{\alpha\beta} = -AQ_{\alpha\beta}$) of the main paper.

Eliminating $R_{\alpha\beta}$ from Eq. (1) using Eq. (2) we find

$$-\nabla p + 2\left(\eta - \frac{2\mu(\mu + \mu_1)}{\nu}\right)\nabla \cdot \mathbf{e} + \left(a - \frac{2(\mu + \mu_1)A}{\nu}\right)\nabla \cdot \mathbf{Q} = 0. \quad (3)$$

To leading order Eq. (2) becomes [using Eq. (3) of the main paper]

$$\partial_t \mathbf{Q} = -\frac{1}{\nu}(A\mathbf{Q} + 2\mu\mathbf{e}). \quad (4)$$

Applying the operations $\nabla \cdot (\nabla \cdot \)$ and $\nabla \times (\nabla \cdot \)$ to Eq. (4), we find

$$\partial_t X = -\frac{A}{\nu}X \quad (5)$$

$$\partial_t \mathbf{Y} = -\frac{A}{\nu}\mathbf{Y} - \frac{2\mu}{\nu}\nabla \times (\nabla \cdot \mathbf{e}), \quad (6)$$

where $X = \nabla \cdot (\nabla \cdot \mathbf{Q})$ and $\mathbf{Y} = \nabla \times (\nabla \cdot \mathbf{Q})$. Taking the curl of Eq. (3) yields

$$2\left(\eta - \frac{2\mu(\mu + \mu_1)}{\nu}\right)\nabla \times (\nabla \cdot \mathbf{e}) + \left(a - \frac{2(\mu + \mu_1)A}{\nu}\right)\mathbf{Y} = 0. \quad (7)$$

Eliminating $\nabla \times (\nabla \cdot \mathbf{e})$ from Eq. (6) using Eq. (7), we obtain

$$\partial_t \mathbf{Y} = -\frac{A\eta - a\mu}{\eta\nu - 2\mu(\mu + \mu_1)}\mathbf{Y}. \quad (8)$$

Eqs. (5) and (8) yield the growth rates shown in Eqs. (12) and (13) of the main paper (using the definitions of the effective viscosities given by Eqs. (6) and (7) of the main paper) and indicate that the mode describing the dynamics of $\nabla \cdot (\nabla \cdot \mathbf{Q})$ always decays with time, whereas the mode describing the dynamics of $\nabla \times (\nabla \cdot \mathbf{Q})$ can grow with time if the factor $-(A\eta - a\mu)/(\eta\nu - 2\mu(\mu + \mu_1))$ is positive.

II. NEXT ORDER TERM IN SWIMMING SPEED U

To find the form of the correction in ϵ to the leading order expression for the swimming speed shown in Eq. (19) of the main paper, we consider the general form of the solution to the equations of motion (1) and (2) of the previous section with the boundary conditions specified in the main paper. The solution has the following form:

$$\begin{aligned} \phi = & \sum_{n=1,3,5\dots}^{\infty} \sum_{m=1,3,5\dots}^n \epsilon^n \phi^{(n,m)}(y) \exp(mi(qx - \omega t)) \\ & + \sum_{n=0,2,4\dots}^{\infty} \sum_{m=0,2,4\dots}^n \epsilon^n \phi^{(n,m)}(y) \exp(mi(qx - \omega t)), \end{aligned} \quad (9)$$

where ϕ denotes ψ , $Q_{\alpha\beta}$, p , and the nonlinear part of $R_{\alpha\beta}$, $N_{\alpha\beta} = \mathbf{v} \cdot \nabla Q_{\alpha\beta} + \omega_{\alpha\gamma} Q_{\gamma\beta} - Q_{\alpha\gamma} \omega_{\gamma\beta}$. Inserting these forms into Eqs. (1) and (2) we obtain, after some straightforward calculation,

$$\psi^{(n,m)}(y) = (C_1 + C_2 y) \exp(-mqy) + \frac{2A\mu_{\text{eff}}}{A\eta_{\text{eff}} + im\omega(2\mu\mu_{\text{eff}} - \eta_{\text{eff}}\nu)} M^{(n,m)}(y), \quad (10a)$$

$$\begin{aligned} Q_{xx}^{(n,m)}(y) = & \frac{-1}{A - im\nu\omega} \left(\nu N_{xx}^{(n,m)}(y) + 2imq\mu \left((C_2(1 - mqy) - C_1mq) \exp(-mqy) \right. \right. \\ & \left. \left. + \frac{2A\mu_{\text{eff}}}{A\eta_{\text{eff}} + im\omega(2\mu\mu_{\text{eff}} - \eta_{\text{eff}}\nu)} DM^{(n,m)}(y) \right) \right), \end{aligned} \quad (10b)$$

$$\begin{aligned} Q_{xy}^{(n,m)}(y) = & \frac{-1}{A - im\nu\omega} \left(\nu N_{xy}^{(n,m)}(y) + \left(2mq\mu(C_2(-1 + mqy) + C_1mq) \exp(-mqy) \right. \right. \\ & \left. \left. + \frac{2A\mu_{\text{eff}}}{A\eta_{\text{eff}} + im\omega(2\mu\mu_{\text{eff}} - \eta_{\text{eff}}\nu)} (D^2 + m^2q^2) M^{(n,m)}(y) \right) \right), \end{aligned} \quad (10c)$$

where C_1 and C_2 are constants which depend on n and m , and

$$M^{(n,m)}(y) = \frac{-1}{(D - mq)^2(D + mq)^2} (m^2q^2 N_{xy}^{(n,m)}(y) + 2imqD N_{xx}^{(n,m)}(y) + D^2 N_{xy}^{(n,m)}(y)). \quad (11)$$

Here $D \equiv \frac{d}{dy}$ and the operator $1/(D \pm mq)$ is defined as

$$\frac{1}{D \pm mq} H(y) = \exp(\mp mqy) \int \exp(\pm mqy) H(y) dy, \quad (12)$$

where $H(y)$ is an arbitrary function. Note that the n^{th} order nonlinear term $N_{\alpha\beta}^{(n,m)}$ is obtained from the sum of the products of lower order terms linear in $\psi^{(k,m)}(y)$, $Q_{\alpha\beta}^{(k,m)}(y)$ ($k < n$) and their derivatives. The first order terms in $N_{\alpha\beta}$ are zero. Therefore $N_{\alpha\beta}^{(1,1)}(y) = M^{(1,1)}(y) = 0$, and $\psi^{(1,1)}(y)$ and $Q_{\alpha\beta}^{(1,1)}(y)$ are independent of $(a_c - a)$. The second order

terms in $N_{\alpha\beta}$ are second order in $\psi^{(1,1)}(y)$, $Q_{\alpha\beta}^{(1,1)}(y)$ and their derivatives. Since $\psi^{(1,1)}(y)$ and $Q_{\alpha\beta}^{(1,1)}(y)$ don't depend on $(a_c - a)$, $N_{\alpha\beta}^{(2,0)}(y)$, $M^{(2,0)}(y)$, $N_{\alpha\beta}^{(2,2)}(y)$ and $M^{(2,2)}(y)$ are also independent of a . Therefore, we can see from the Eq. (10) (recalling $\eta_{\text{eff}} = \mu(a_c - a)/A$) that $Q_{xx}^{(2,0)}(y)$ is independent of $(a_c - a)$, and $\psi^{(2,2)}(y)$, $Q_{xx}^{(2,2)}(y)$ and $Q_{xy}^{(2,2)}(y)$ approaching a finite limit and

$$\psi^{(2,0)}(y), Q_{xy}^{(2,0)}(y) \rightarrow \frac{1}{(a_c - a)^1} \quad \text{as} \quad a \rightarrow a_c. \quad (13)$$

The third order terms in $N_{\alpha\beta}$ arise due to the products of $d\phi^{(1,m)}(y)/dy^k$ and $d\phi^{(2,m)}(y)/dy^k$, where $k = 0, 1, 2$ and ϕ stands for ψ and $Q_{\alpha\beta}$. Thus, from (13),

$$N_{\alpha\beta}^{(3,1)}(y), M^{(3,1)}(y), N_{\alpha\beta}^{(3,3)}(y), M^{(3,3)}(y) \rightarrow \frac{1}{(a_c - a)^1} \quad \text{as} \quad a \rightarrow a_c. \quad (14)$$

Hence

$$\psi^{(3,1)}(y), Q_{\alpha\beta}^{(3,1)}(y), \psi^{(3,3)}(y), Q_{\alpha\beta}^{(3,3)}(y) \rightarrow \frac{1}{(a_c - a)^1} \quad \text{as} \quad a \rightarrow a_c. \quad (15)$$

The fourth order term in $N_{\alpha\beta}$ are the linear combinations of $d\phi^{(n_1,m)}(y)/dy^k d\phi^{(n_2,m)}(y)/dy^k$, where $k = 0, 1, 2$, $n_1 + n_2 = 4$ and ϕ stands for ψ and $Q_{\alpha\beta}$. Thus, from (13) and (15),

$$\begin{aligned} N_{\alpha\beta}^{(4,0)}(y), M^{(4,0)}(y), N_{\alpha\beta}^{(4,2)}(y), \\ M^{(4,2)}(y), N_{\alpha\beta}^{(4,4)}(y), M^{(4,4)}(y) \rightarrow \frac{1}{(a_c - a)^2} \quad \text{as} \quad a \rightarrow a_c. \end{aligned} \quad (16)$$

Hence

$$\psi^{(4,0)}(y) \rightarrow \frac{1}{(a_c - a)^3} \quad \text{as} \quad a \rightarrow a_c. \quad (17)$$

Above analysis suggests that ψ and $Q_{\alpha\beta}$ can be written in terms of the inverse power series of $a_c - a$, starting with the terms independent of that quantity.

Since we have $\epsilon \rightarrow -\epsilon$ symmetry, the next order correction to U will be $\epsilon^4 \partial_y \psi^{(4,0)}(y)$, which goes as $\epsilon^4/(a_c - a)^3$ as $a \rightarrow a_c$. Similarly, the next order term in the power dissipated in the fluid P_F also goes as $\epsilon^4/(a_c - a)^2$. However, the power supplied by the swimmer P_S goes as $\epsilon^4/(a_c - a)$ because the fluid velocity at the Taylor sheet does not depend on $a_c - a$.

III. SIMULATION DETAILS

The typical wavelength of the perturbations near the Taylor sheet is comparable to the wavelength of the sheet (2π in dimensionless units). Thus we need to divide the region close

to the sheet into grids of size much smaller than 2π . Far away from the sheet, the typical wavelength of the perturbations is of the order of the system size along the x direction, which is 32π in dimensionless units. This region far from the sheet can thus be divided into larger grids. To smooth this variation in the grid size from the region near the sheet to the region near the bounding wall, we divided the simulation box into 4 subboxes along the y direction, the direction perpendicular to the flat Taylor sheet (see Fig. 1). Each subbox is divided into triangular grids of different sizes, determined automatically by COMSOL after we input the maximum grid size. The sizes of the subboxes, the number of triangular grids in each subbox and the maximum size of the grids (i.e., the length of the sides of the triangles) are shown in the following table:

	Size of the subbox	No. of grids	Maximum grid size
Subbox I	$32\pi \times 6$	15382	0.314
Subbox II	$32\pi \times 6$	6736	1.26
Subbox III	$32\pi \times 12$	1976	2.51
Subbox IV	$32\pi \times 36$	944	5.03

The Taylor sheet is represented by the top deformable wall of the simulation box; subbox I is adjacent to the sheet and subbox IV is at the bottom of the simulation box. Since small wavelength perturbations are important close to the Taylor sheet, subboxes I and II are divided into numerous small grids compared to subboxes III and IV.

IV. SWIMMING SPEED CALCULATION FOR THE SQUIRMER

We consider a cylindrical squirmer [1] of radius R subject to surface waves defined in polar coordinates by

$$r = R[1 + \epsilon\Delta r], \quad (18)$$

$$\phi = \theta + \epsilon\Delta\theta, \quad (19)$$

where

$$\Delta r = \Delta_1 \cos \omega t \cos N\theta + \Delta_2 \sin \omega t \cos(N + 1)\theta, \quad (20)$$

$$\Delta\theta = \Delta_3 \cos \omega t \sin N\theta + \Delta_4 \sin \omega t \sin(N + 1)\theta, \quad (21)$$

where the Δ_i are dimensionless numbers.

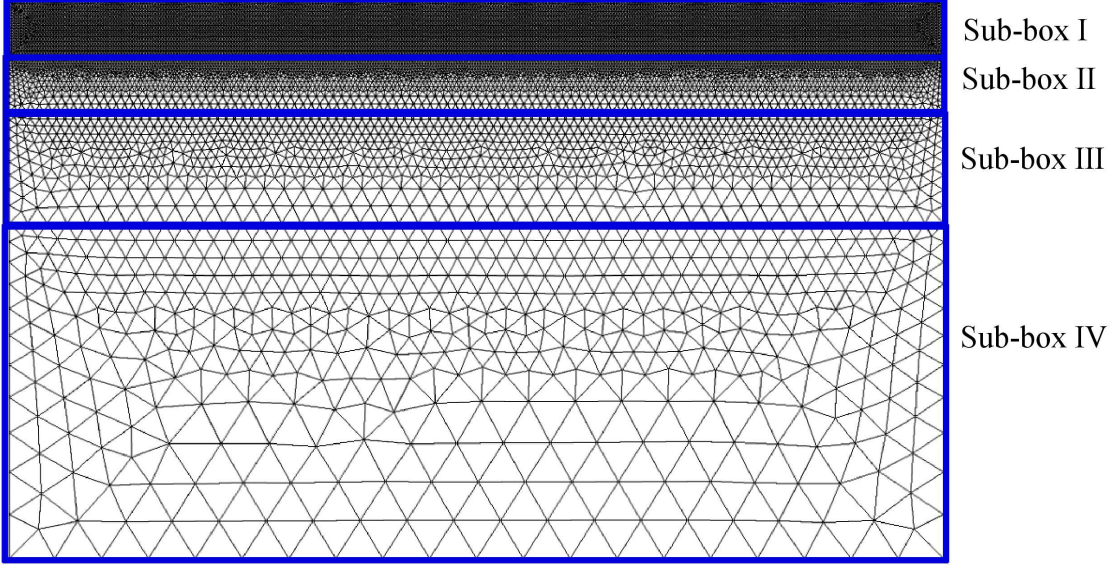


FIG. 1: (Color online.) The rectangular simulation box of size $32\pi \times 16$ is divided into four subboxes. Each subbox is further divided into triangular grids.

We assume that $\epsilon \ll 1$. As in the case of the Taylor sheet, we use no slip boundary conditions at the surface of the squirmer. The radial and azimuthal components of the velocity field at the surface of the squirmer are then given by:

$$v_\rho(\rho = r, \theta = \phi) = \dot{r} = \epsilon R \omega (-\Delta_1 \sin \omega t \cos N\theta + \Delta_2 \cos \omega t \cos(N+1)\theta), \quad (22)$$

$$v_\theta(\rho = r, \theta = \phi) = r\dot{\phi} = R[1 + \epsilon(\Delta_1 \cos \omega t \cos N\theta + \Delta_2 \sin \omega t \cos(N+1)\theta)] \\ \times \epsilon \omega (-\Delta_3 \sin \omega t \sin N\theta + \Delta_4 \cos \omega t \sin(N+1)\theta). \quad (23)$$

In polar coordinates the velocity components are related to the stream function ψ by

$$v_\rho = \frac{1}{\rho} \frac{d\psi}{d\theta}, v_\theta = -\frac{d\psi}{d\rho}, \quad (24)$$

We expand ψ , $Q_{\alpha\beta}$ and U in ϵ :

$$\psi = \psi^{(1)}\epsilon + \psi^{(2)}\epsilon^2 \dots \quad (25)$$

$$Q_{\alpha\beta} = Q_{\alpha\beta}^{(1)}\epsilon + Q_{\alpha\beta}^{(2)}\epsilon^2 \dots \quad (26)$$

$$U = U^{(1)}\epsilon + U^{(2)}\epsilon^2 \dots \quad (27)$$

The boundary conditions (22) and (23) yield to first order in ϵ

$$\left. \frac{d\psi^{(1)}}{d\theta} \right|_{(R,\theta)} = R^2 \frac{d\Delta r}{dt} \quad (28)$$

$$\left. \frac{d\psi^{(1)}}{d\rho} \right|_{(R,\theta)} = R \frac{d\Delta\theta}{dt} \quad (29)$$

and to second order

$$\left. \frac{d\psi^{(2)}}{d\theta} \right|_{(R,\theta)} = \left[\frac{d\psi^{(1)}}{d\theta} - R \frac{d^2\psi^{(1)}}{d\rho d\theta} \right]_{(R,\theta)} \Delta r - \left. \frac{d^2\psi^{(1)}}{d\theta^2} \right|_{(R,\theta)} \Delta\theta \quad (30)$$

$$\left. \frac{d\psi^{(2)}}{d\rho} \right|_{(R,\theta)} = -R\Delta r \left[\left. \frac{d^2\psi^{(1)}}{d\rho^2} \right|_{(R,\theta)} + \frac{d\Delta\theta}{dt} \right] - \left. \frac{d^2\psi^{(1)}}{d\rho d\theta} \right|_{(R,\theta)} \Delta\theta. \quad (31)$$

The boundary conditions at infinity are given by

$$\nabla \times (\psi^{(1)} \hat{\mathbf{z}})|_{(\infty,\theta)} = U^{(1)} \cos \theta \hat{\boldsymbol{\rho}} - U^{(1)} \sin \theta \hat{\boldsymbol{\theta}} \quad (32)$$

$$\nabla \times (\psi^{(2)} \hat{\mathbf{z}})|_{(\infty,\theta)} = U^{(2)} \cos \theta \hat{\boldsymbol{\rho}} - U^{(2)} \sin \theta \hat{\boldsymbol{\theta}} \quad (33)$$

The first order terms in ψ and $Q_{\alpha\beta}$ have the following form:

$$\psi^{(1)} = \sum_{s_1, s_2 = \pm 1} \sum_{n=N}^{N+1} \psi_0^{(1)}(\rho, n, s_1, s_2) \exp(s_1 n \theta + s_2 \omega t) \quad (34a)$$

$$Q_{\rho\rho}^{(1)} = \sum_{s_1, s_2 = \pm 1} \sum_{n=N}^{N+1} Q_{\rho\rho 0}^{(1)}(\rho, n, s_1, s_2) \exp(s_1 n \theta + s_2 \omega t) \quad (34b)$$

$$Q_{\rho\theta}^{(1)} = \sum_{s_1, s_2 = \pm 1} \sum_{n=N}^{N+1} Q_{\rho\theta 0}^{(1)}(\rho, n, s_1, s_2) \exp(s_1 n \theta + s_2 \omega t) \quad (34c)$$

Solving Eq. (2) to first order with the form of the first order solutions given in Eqs. (34), we find

$$Q_{\rho\rho 0}^{(1)} = \frac{2n s_1 \mu}{(iA - s_2 \omega \nu)} \left[\frac{1}{\rho} \frac{d\psi_0^{(1)}}{d\rho} - \frac{1}{\rho^2} \psi_0^{(1)} \right] \quad (35)$$

$$Q_{\rho\theta 0}^{(1)} = \frac{i\mu}{iA - s_2 \omega \nu} \left[\frac{n^2 s_1^2}{\rho^2} \psi_0^{(1)} - \frac{1}{\rho} \frac{d\psi_0^{(1)}}{d\rho} + \frac{d^2\psi_0^{(1)}}{d\rho^2} \right] \quad (36)$$

Taking the curl of Eq. (1) and then substituting the above values of $Q_{\rho\rho 0}^{(1)}$ and $Q_{\rho\theta 0}^{(1)}$ yields to first order

$$\left[\rho^4 \frac{d^4}{d\rho^4} + 2\rho^3 \frac{d^3}{d\rho^3} - (1 + 2n^2 s_1^2) \rho^2 \frac{d^2}{d\rho^2} + (1 + 2n^2 s_1^2) \rho \frac{d}{d\rho} + n^2 s_1^2 (-4 + n^2 s_1^2) \right] \psi_0^{(1)} = 0 \quad (37)$$

The finite value solutions of the above equation have the form

$$\psi_0^{(1)} = A_1(n, s_1, s_2) \rho^{-n} + A_2(n, s_1, s_2) \rho^{2-n} \quad (38)$$

where $A_i(n, s_1, s_2)$, $i = 1, 2$ are the constants. With the boundary conditions (28) and (29), we find

$$\psi^{(1)} = \mathcal{A}_1(\rho) \sin \omega t \sin N\theta + \mathcal{A}_2(\rho) \cos \omega t \sin(N+1)\theta$$

$$Q_{\rho\rho}^{(1)} = \mathcal{A}_3(\rho)(\nu\omega \cos \omega t - A \sin \omega t) \cos N\theta + \mathcal{A}_4(\rho)(A \cos \omega t + \nu\omega \sin \omega t) \cos(N+1)\theta$$

$$Q_{\rho\theta}^{(1)} = \mathcal{A}_3(\rho)(\nu\omega \cos \omega t - A \sin \omega t) \sin N\theta + \mathcal{A}_4(\rho)(A \cos \omega t + \nu\omega \sin \omega t) \sin(N+1)\theta$$

where

$$\mathcal{A}_1(\rho) = \frac{(\Delta_3 - \Delta_1)N(\rho/R)^2 + \Delta_1(N-2) - \Delta_3N}{2N} \left(\frac{\rho}{R}\right)^{-N} \quad (39)$$

$$\mathcal{A}_2(\rho) = \frac{(\Delta_2 - \Delta_4)(N+1)(\rho/R)^2 + \Delta_4(N+1) - \Delta_2(N-1)}{2(N+1)} \left(\frac{\rho}{R}\right)^{-N-1} \quad (40)$$

$$\mathcal{A}_3(\rho) = \frac{\mu[-(N+1)(N-2)\Delta_1 + N(N+1)\Delta_3 + N(N-1)(\Delta_1 - \Delta_3)(\rho/R)^2]}{A^2 + \nu^2\omega^2} \left(\frac{\rho}{R}\right)^{-N-2} \quad (41)$$

$$\mathcal{A}_4(\rho) = \frac{\mu[-(N-1)(N+2)\Delta_2 + (N+1)(N+2)\Delta_4 + N(N+1)(\Delta_2 - \Delta_4)(\rho/R)^2]}{A^2 + \nu^2\omega^2} \left(\frac{\rho}{R}\right)^{-N-3} \quad (42)$$

We use the above first order solutions in the second order forms of Eqs. (1) and (2) and solve these equations using Mathematica with the following result for the swimming speed to second order:

$$U = U_0 + \frac{1}{8}\epsilon^2 R\omega \left[\frac{2\nu\mu\mu_{\text{eff}}\omega^2}{\eta_{\text{eff}}(A^2 + \nu^2\omega^2)} \right] \mathcal{G} \quad (43)$$

where

$$\begin{aligned} \mathcal{G} = & \frac{\Delta_1\Delta_2(N(N(N(2N+11)+3)-26)-10) - \Delta_2\Delta_3(N(N(N(2N+11)+10)-6)+3)}{(N+1)(N+2)(N+3)} \\ & - \frac{\Delta_4(N+1)(\Delta_1(N+1)(N+4)(2N+1) + \Delta_3(N(N+2)(2N+5)-3))}{(N+1)(N+2)(N+3)} \end{aligned} \quad (44)$$

and U_0 is the speed of the squirmer in the Newtonian fluid:

$$U_0 = \frac{1}{8}\epsilon^2 R\omega [\Delta_4(2N+1)(\Delta_1 + \Delta_3) - \Delta_2(\Delta_3 + \Delta_1(2N-3) - 2\Delta_3N)]. \quad (45)$$

One can see from the above expression for the swimming speed U that the change in the swimming speed due to anisotropy is proportional to $2\nu\mu\mu_{\text{eff}}\omega^2/\eta_{\text{eff}}(A^2 + \nu^2\omega^2)$ which is qualitatively similar to the result obtained for the Taylor sheet [see Eq. (19) of the main article].

[1] J. R. Blake, *J. Fluid Mech.* **46**, 199 (1971).